MECHANISTIC INSIGHTS ON ENVIRONMENTAL DEGRADATION FROM NANOMETER-SCALE CRACK-TIP MEASUREMENTS

S. M. BRUEMMER & L. E. THOMAS
Pacific Northwest National Laboratory
Richland, Washington 99352 USA

ABSTRACT

Mechanisms controlling environmental degradation and cracking in light-water-reactor (LWR) systems have been investigated by analytical transmission electron microscopy (ATEM) of cracks and crack tips. The current work focuses on intergranular stress corrosion cracking (IGSCC) of 300-series, austenitic stainless steels in high-temperature LWR environments. Comparisons are made between cold-worked 304SS containing stress-corrosion cracks produced in a simulated boiling-water-reactor (BWR) environment during crack-growth tests, and a 304SS core component with cracks produced during 26-year BWR service. Similar corrosion products consisting of duplex-layered spinel oxides were found along the walls of open cracks in the service and laboratory test samples. These oxide films consisted of oriented Cr-rich spinel up to ~30 nm thick along the metal crack walls and large-grained Fe-rich spinel at the crack centers. Cracks in the service sample were generally more filled with oxide, perhaps reflecting the much longer times available for corrosion to occur after the crack passage. Crack tips in the BWR top-guide sample exhibited unique and unexpected structures with oxide-filled cracks <10 nm wide ending in finger-like attack and locally "dealloyed" zones of Fe/Cr-depleted, Ni-rich metal. Alloy compositions measured at numerous crack tips were 40 wt% Fe, 4 wt% Cr and 55 wt% Ni immediately ahead of the degradation front versus approximately 70 wt% Fe, 19 wt% Cr and 9 wt% Ni in the bulk 304SS. Laboratory samples with cracks grown over much shorted times (~1.5 months) did not show the distinctive crack tip structures or strong Ni enrichment in the metal ahead of the crack tips as for the service sample. This suggests that although selective oxidation processes occur during degradation, significant composition differences may only develop after crack propagation has slowed or stopped. Additional nanometer-scale measurements elucidating corrosion processes occurring during crack advance are presented to provide insights into mechanisms controlling IGSCC.

1 INTRODUCTION

The fundamental basis for mechanistic understanding and modeling of stress corrosion cracking (SCC) remains in question for many systems. Specific mechanisms controlling SCC can vary with changes in alloy characteristics, applied/residual stress or environmental conditions. The local crack electrochemistry, crack-tip mechanics and material metallurgy are the main factors controlling crack growth. These localized properties are difficult or impossible to measure in active cracks. Nevertheless, it is essential to quantitatively interrogate these crack-tip conditions if mechanistic understanding is to be obtained.

A major recent advance has been the ability to investigate SCC cracks and crack tips using analytical transmission electron microscopy (ATEM). ATEM enables the characterization of trapped solution chemistries, corrosion product compositions and structures, composition gradients and defect microstructures along the crack walls and at the crack tip. A wide variety of methods for imaging and analyses at resolutions down to the nanometer scale and below can be used to examine the crack and corrosion film characteristics. A critical aspect of the recent work [1-7] has been the development of sample preparation methods in which the crack corrosion products are protected during the ion-thinning process by embedding the cracks with a low-viscosity thermoplastic resin. This capability combined with modern ATEM techniques has enabled new insights into corrosion processes occurring at crack tips and is being used to identify mechanisms controlling SCC in service components. A key aspect has been direct comparisons between service components with cracks produced under complex, historically varied conditions and well-controlled laboratory test samples.

The objective of this brief paper is to highlight new results focused on intergranular (IG) SCC in austenitic stainless steels comparing cracks produced in boiling-water-reactor (BWR) service and those produced during laboratory crack-growth tests in a simulated BWR water environment. Examples are chosen to illustrate nanometer-scale structures that can only be examined effectively by ATEM methods.

2 MATERIALS, SAMPLE PREPARATION AND CHARACTERIZATION APPROACH

The service-component cracked samples were removed from a Type 304SS top guide in the Oyster Creek BWR after ~26 years in service [8]. Cracks initiated at the bottom of the egg-crate upper beams (9.1-mm thick plate) in the higher flux region facing the reactor core. A small section containing the crack and crack-tip was removed and retrospective dosimetry determined that the radiation dose at this location was ~0.7 dpa. The crack-growth testing was performed at General Electric Global Research on a 20% cold-worked Type 304SS in a simulated BWR environment at 288^{o}C [9]. The test was stopped after ~0.5-mm of IGSCC crack extension at a constant K (33 MPa$\sqrt{m}$) with an average crack-growth rate of 1.4×10^{-7} mm/s. Crack opening was maintained during removal from the test system and wedged for shipment to Pacific Northwest National Laboratory for preparation.

Cross-section crack samples for ATEM characterization were prepared much as described earlier [3,4]. In brief, small pieces containing selected crack tips were cut from metallographically polished samples following vacuum impregnation with a low-viscosity thermosetting resin. The small slices were then glued to 3-mm-diameter Mo washers (the size of a TEM disk), with the crack tips at the disk centers. After trimming edges and flat polishing to ~100 µm total thickness, the samples were dimple-ground from the washer sides and finished by low-angle ion micromilling with 2 to 5 KeV argon ions. Repeated cycles of ion thinning and TEM examination were used to obtain suitably thin areas at crack tips or other locations of interest. ATEM characterizations were performed using a 200 kV field-emission-gun TEM with a thin-window, energy-dispersive x-ray spectrometer (EDS) and a parallel-detection electron-energy-loss spectrometer (PEELS) for microchemical analysis. Besides conventional brightfield and precipitate darkfield imaging, characterization methods included crystal lattice imaging with Fourier-transform diffraction analysis, fine-probe (0.7-nm diameter) compositional analysis by EDS and PEELS, and fine-probe parallel-beam diffraction with electron probes as small as 5 nm in diameter. In addition, stereoscopic TEM photographs were used to observe finely porous structures along attacked grain boundaries. A Fresnel (off-focus) image contrast method was employed to reveal fine pores and other structures as small as 1 nm.

3 RESULTS AND DISCUSSION

3.1 Crack and Crack-Wall Structures

TEM examinations of cracks in the BWR top-guide material included multiple branch cracks up to a distance of ~0.5 mm behind the furthest advanced tip. The corrosion products in cracks consisted of uniform thin films of dense, epitaxial Fe-Cr-Ni spinel (Cr enriched relative to the metal matrix) next to the metal and Fe-rich spinel toward the crack centers. Open gaps between the oxide layers appeared in cracks wider than ~100 nm. The oxide-filled cracks continued over distances of tens of µm along all the intersected grain boundaries off major cracks, and the cracks tapered very gradually to the tips. As cracks narrowed, the width of the central magnetite layer gradually decreased until only the Cr-rich inner oxide remained. Figure 1(a) schematically illustrates the corrosion structures in the oxide-filled cracks and emphasizes the gradual tapering and regularity of the cracks as they narrow toward their tips. Major characteristics of the crack-wall structures were thin layers of crystallographically oriented spinel along the metal/oxide interfaces and elongated Fe-rich spinel grains filling the cracks between the Cr-rich spinel layers. Fine porosity (~2- to 5-nm-diameter cavities) appeared along the metal/oxide interfaces at distances greater than ~500 nm behind the acute crack tips, but the interfacial porosity was generally absent near the tips. An example of the crack and crack-wall structures many µm behind the crack front is shown in Figure 1(b). The microstructure in this area consisted of an essentially single-crystal layer of Fe-rich spinel (magnetite) bounded by narrow layers of epitaxial Cr-rich spinel along porous, rough metal oxide interfaces. Although this micrograph shows the metal/oxide interfaces slightly inclined to the viewing direction, tilting the sample to view the structures edge-on indicated the porosity was actually at the interfaces. Minor fine cavities also appeared aligned in lines or sheets within the Fe-rich spinel, apparently due to preferential formation of the cavities along dislocations or other internal defects in the oxide. EDS analyses showed traces of S throughout the oxide of this area, and EELS analysis further indicated Mn in the oxide. Figure 2(a) shows the oxide structure in a narrow crack only ~20 nm wide. As in the previous example, oxide filled the available volume. In areas such as this, the cracks characteristically contained oxide layers with nearly planar, nonporous metal/oxide interfaces. EDS composition profiles given in Figure 2(b) reveal the narrow Cr-rich inner oxide and Fe-rich center layer along with Cu and Ni enrichment at m/o interfaces.

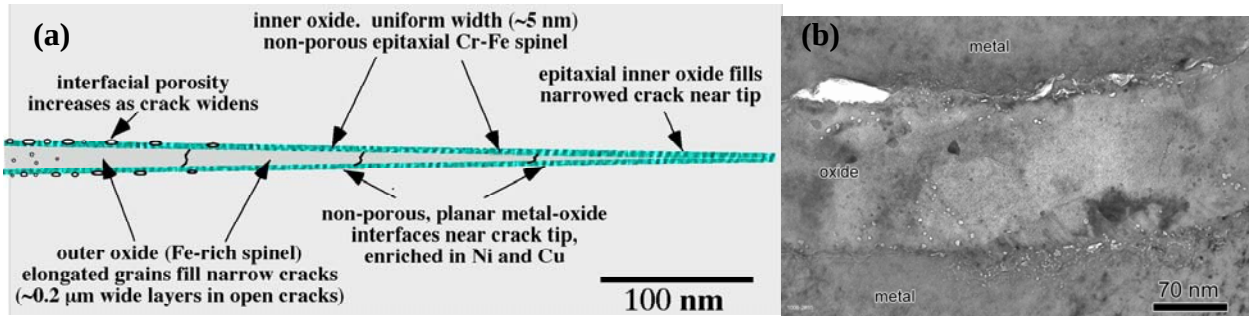

Figure 1. Oxide-filled cracks in BWR top-guide material: (a) schematic illustrating crack structure as it approaches the tip and (b) TEM brightfield image showing magnetite-filled crack region ~15 µm behind the crack tip.

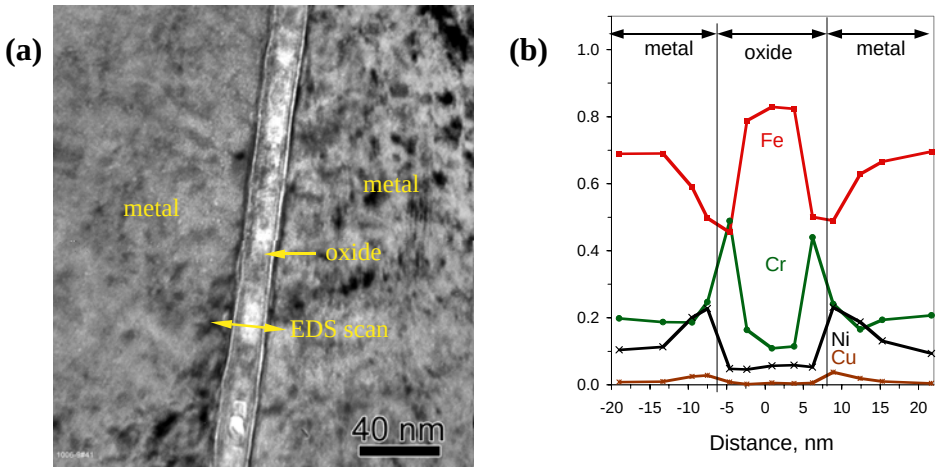

Figure 2. Narrow oxide-filled crack near a crack tip in the top-guide sample: (a) TEM brightfield image and (b) fine-probe compositional profile showing Fe-rich oxide in center of crack and Cr-rich oxide at crack walls.

Cracks and crack oxide structures in the laboratory crack-growth sample were generally similar to the service sample even though the exposure times to 288°C water was quite different. Once again, epitaxial Cr-rich spinel was seen next to the metal and Fe-rich spinel in the crack centers as illustrated in Figure 3. Unlike the cracks in the service sample, many cracks produced in the laboratory test sample contained open central gaps that had become filled with epoxy during the preparation. In some cases, the cracks appeared open nearly to the tips. The narrow Cr-rich spinel layers along the crack walls continued all the way to the tips. As shown by a compositional profile in Figure 3(b), minor Ni and Cu enrichments occurred at the metal/oxide interfaces.

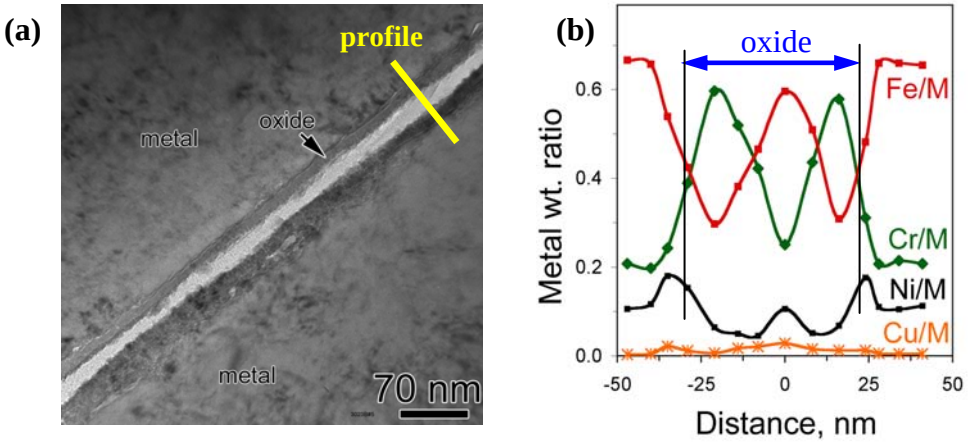

Figure 3. Oxide-filled crack about 1µm behind tip in the laboratory sample: (a) TEM brightfield image showing bi-layer film and (b) compositional profile showing Fe-rich oxide in center of crack and Cr-rich oxide at crack walls.

3.2 Crack-Tip Structures

Extensive crack branching in this BWR top-guide material produced numerous crack tips for detailed TEM analysis. Nearly all crack tips examined in detail had the following characteristics in common. The oxide-filled cracks gradually tapered over many μm to end at "expanded" porous tips at the metal grain boundary. For example, the oxide-fill width decreased from ~35 nm to ~15 nm over the final μm leading up to the crack tip. Porous-tip structures are illustrated in Figures 4(a) and 4(b) showing the oxide fill ending immediately behind the actual tip. Another distinctive characteristic of most tips was a marked deflection of the grain boundaries just ahead of the tips as seen in Figure 4. Most tips also exhibited distinctive finger-like porous structures at their ends. In order to better elucidate this structure at the tips, Fresnel-contrast imaging was obtained from edge-on and inclined views in Figure 5. Finger-like porosity can clearly be seen along the attack interfaces into the metal beyond the corrosion-product oxide. These pores were generally elongated in the growth direction, and had ~10 nm equiaxed diameters and ~10-nm inter-pore spacings. Stereo pairs were recorded confirming the 3-dimensional porosity of the tip structures both in the leading edge metal and in the oxide.

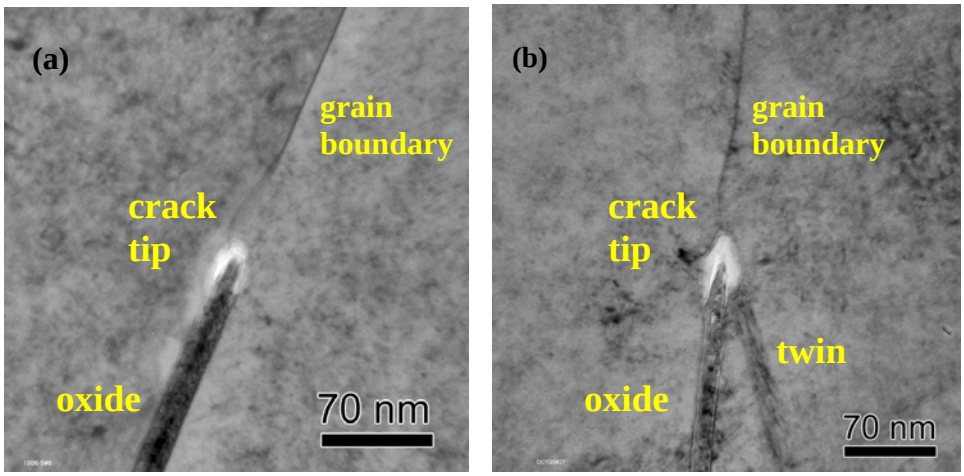

Figure 4. TEM images showing two crack tips in the BWR top guide sample: (a) narrow oxide-filled crack over last μm leading to tip, insets show details of porous tip and oxide-filled crack; (b) and (c) document typical crack tip appearance with oxide ending in a porous region and grain boundary deviation immediately ahead of tip.

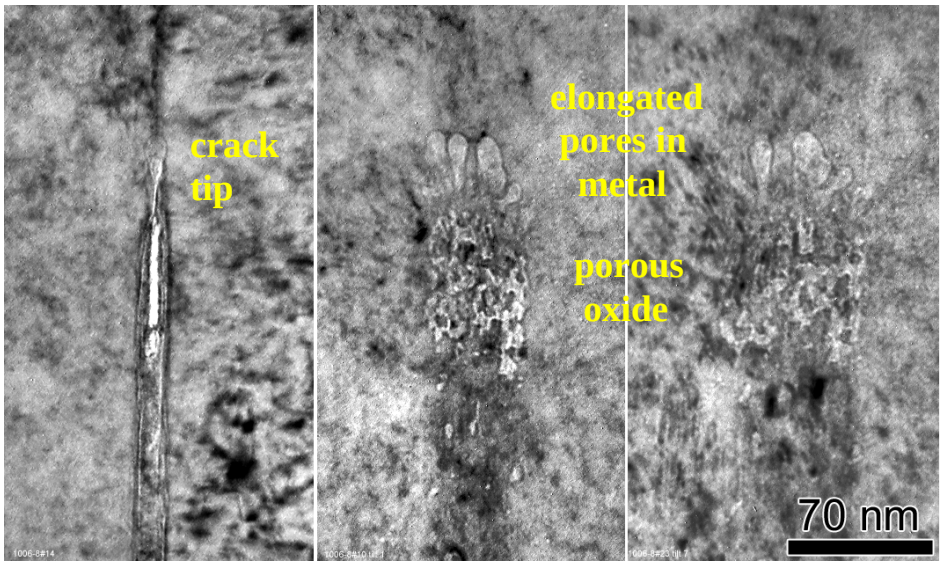

Figure 5. Crack tip shown at 3 tilt inclinations using underfocus TEM brightfield: (a) crack edge-on at 0°, (b) crack inclined by 30° and (c) inclined by 45°.

Another important crack-tip characteristic was the altered metal composition leading the tips. Fine-probe EDS analyses of the tip region revealed highly Ni-rich metal regions ~10-nm wide and ~40-nm long just ahead of the tip. Composition profiles revealed that the cracks ended in a region with a composition of approximately 40Fe-4Cr-55Ni quite different than that for the stainless steel matrix (71Fe-18Cr-9Ni) or the segregated grain boundary (64Fe-16Cr-18Ni-2Si). The highest Ni concentrations occurred ~5 nm off the grain boundary, and the boundary appeared locally deviated (see Figure 4) at the Ni-rich region. Composition profiles show that the region adjacent to the migrated grain boundary, and not the grain boundary itself, exhibits the most significant change in composition. At ~120 nm ahead (of the tip, the composition drops back to a level typical of the bulk alloy in this irradiated material.

Structures and local compositions were quite different at the crack tips in the laboratory sample. The bi-layer oxide continued to ~100 nm behind the tips then transitioned to only Cr-rich spinel similar to the service cracks. However, the dense, oriented oxide on the crack walls continued to the tips, and there was no evidence of porous oxide or Ni-rich metal at the tip as seen in Figures 4 and 5 for the service sample. An example of a tip region is shown in Figure 6. Extensive deformation structure is present throughout along with evidence of local shear bands intersecting the crack walls and grain boundaries in metal. Fine-probe EDS measurements have not found any significant compositional change (e.g., Fe/Cr depletion and Ni enrichment) in the metal immediately ahead of the crack tip.

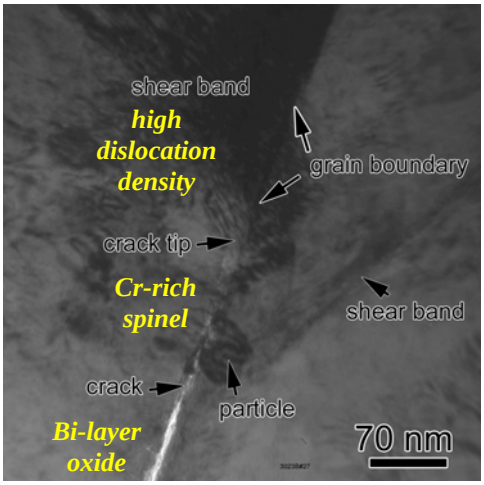

Figure 6. TEM image showing a oxide-filled crack tip in the laboratory crack-growth sample.

The application of high-resolution ATEM methods to crack corrosion interfaces and crack tips in stress-corrosion cracked stainless steels has revealed important details of the degradation processes and mechanisms. This advance comes from two developments: (1) improvements in cross-sectional sample preparation on cracked materials, and (2) the availability of FEG TEMs that allow structural, compositional and crystallographic analyses at resolutions down to atomic dimensions. The formation of bi-layer corrosion-product films in SCC cracks for the service and laboratory samples is in general agreement with surface films reported on stainless steels after high-temperature water exposure [10,11]. A thin Cr-rich oxide on the crack walls and at crack tips is consistent with a classical SCC slip-oxidation mechanism. Localized breakdown of the protective film at the tip prompts further oxidation at/near leading grain boundary and IG crack extension. These steps would be expected to produce the crack wall and tip films seen in the laboratory crack-growth sample and agree with the high deformation structure (including shear bands) in the general tip region. However, quite different crack-tip structures and compositions have developed in the service sample. Selective dissolution of Fe and Cr has occurred at the crack tip producing an unstable corrosion interface (finger-like attack). Considering the presence of dense oxide filling cracks in the top guide example over long distances up to the tips, and the slow diffusion kinetics of Fe, Ni and Cr in SS at 288^{o}C, it seems likely that the observed cracks in this case were not actively growing. Even if corrosion reactions altered subsurface diffusion rates by H or vacancy injection [12], the depth of the composition change (~100 nm) suggests that the tip must have been stationary for considerable time. In the laboratory sample with active crack growth, no evidence of selective dissolution was found. A final observation worth noting is that crack openings narrow at the tips in both samples to only a few nm. Crack tips were either filled with corrosion product oxide or (in the case of

the laboratory test sample) with the epoxy introduced with the sample still under load. Therefore, the crack-tip openings during active crack propagation appeared to be only a few nm. This characteristic needs to be considered in SCC mechanistic models both for the crack-tip stress and strain-rate aspects, and for the migration of species to the tip reaction front.

This work has demonstrated the ability of ATEM to reveal new and important details of SCC structures that cannot be detected by other methods. However, the current observations must be considered work in progress and additional work is needed to properly establish mechanisms controlling IGSCC. In particular, ATEM characterizations must be performed on samples where mechanisms are better distinguished and controlling variables are systematically varied. Tests are underway in high-temperature aqueous environments under well-controlled solution chemistries and electrochemical conditions to establish a library of SCC signatures.

CONCLUSIONS

Cross-sectional ATEM has been used to characterize SCC cracks and crack tips developed in a BWR component and in a laboratory crack-growth test. A wide variety of high-resolution imaging and analysis methods were employed to elucidate processes occurring during crack advance. Similar crack corrosion films were observed in the two examples, but fundamental differences appeared at crack tips. Local attack ending in de-alloyed metal along leading grain boundaries was observed at tips in the service sample. Crack tips in the laboratory sample did not show a porous structure nor compositionally altered metal ahead of the crack tip. This suggests that some of the crack corrosion characteristics observed in service cases may only develop after crack propagation has slowed or stopped. Results presented demonstrate the ability of cross-sectional ATEM to reveal new details of crack-tip structures that cannot be detected by other methods.

ACKNOWLEDGEMENTS

Primary support comes from the Offices of Basic Energy Sciences and Nuclear Energy, Science & Technology, U.S. Department of Energy under contract DE-AC06-76RLO 1830 with Battelle Memorial Institute. Work on the BWR top guide was also supported by the international Cooperative IASCC Research Program and EPRI.

REFERENCES

1. Lewis, N., Perry, D.J. and Bunch, M.L. (1995) In: *Proc. Microscopy and Microanalysis,* ed., Bailey, G.W. et al., Jones and Begnell Publishing, New York, 550.
2. Lewis, N., Attanasio, S., Morton, D.S. and Young, G.A. (2001) In: *Proc. Staehle Symposium on Chemistry and Electrochemistry of Corrosion and Stress Corrosion*, ed. Jones, R.H. TMS, p. 421.
3. Thomas, L.E., Charlot, L.A. and Bruemmer, S.M. (1996) In: *Proc. New Techniques for Characterizing Corrosion and Stress Corrosion*, Eds. Jones, R.H. and Baer, D.R. TMS, p. 175.
4. Thomas, L.E. and Bruemmer, S.M. (2000) *Corrosion J.*, 56, 572.
5. Thomas, L.E. and Bruemmer, S.M. (2000) In: *Proc. 9th Int. Conf. Environmental Degradation of Materials in Nuclear Power Systems-Water Reactors,* ed. Bruemmer, S.M., Ford, F.P., TMS, p. 41.
6. Bruemmer, S.M. and Thomas, L.E. (2001) In: *Proc. Staehle Symposium on Chemistry and Electrochemistry of Corrosion and Stress Corrosion*, ed. Jones, R.H. TMS, p. 123.
7. Bruemmer, S.M. and Thomas, L.E. (2001) *J. Surface and Interface Analysis*, in press.
8. Thomas, L.E. and Bruemmer, S.M. (2004) In: *Proc. 11th Int. Conf. Environmental Degradation of Materials in Nuclear Power Systems-Water Reactors,* ed. Nelson, J. L., G. S. Was, American Nuclear Society, p. 1049.
9. Andresen, P.L., Young, L.M., W.R. Catlin and R.M. Horn (2004) In: Proc. Corrosion 2004, National Association of Corrosion Engineers, Paper 04678.
10. Robertson, J. (1991) *Corrosion Sci.*, 32-4, 443.
11. Stellwag, B. (1998) *Corrosion Sci.*, 40-2/3 337.
12. Simonen, E.P., Thomas, L.E. and Bruemmer, S.M. (2004) In: *Proc. 11th Int. Conf. Environmental Degradation of Materials in Nuclear Power Systems-Water Reactors*, ed. Nelson, J. L., G. S. Was, American Nuclear Society, p. 1062.